CrystEngComm

Accepted Manuscript

ROYAL SOCIETY OF CHEMISTRY

www.rsc.org/crystengcomm

Journal Name

ARTICLE

A facile method to control the structure and morphology of α-calcium sulfate hemihydrate

Qiaoshan Chen,[a] Guangming Jiang,[b] Caiyun Jia,[a] Hao Wang[a] and Baohong Guan*[a]

Received 00th January 20xx,
Accepted 00th January 20xx

DOI: 10.1039/x0xx00000x

We report a facile method to control the structure and morphology of alpha-calcium sulfate hemihydrate (α-HH) crystals precipitated in Na_2EDTA-contained ethylene glycol aqueous solutions by simply tuning the volume ratio of ethylene glycol to water (G/W). At a low G/W from 0.4 to 2.5, single crystalline α-HH particles with hexagonal prism shape precipitate from the solution, the corresponding aspect ratio of the prisms varies from 2.7 to 0.1. While at a high G/W from 5.0 to 50.0, polycrystalline α-HH particles form with spherical and ellipsoidal shape and the diameter of the polycrystalline spheres reduces from 2 μm to 300 nm. The synergetic effect of supersaturation and Na_2EDTA activity resulted from G/W accounts for the evolution of structure and morphology of α-HH. This method allows α-HH synthesis in micro and nanoscale size, thus enabling its morphology/structure-dependent applications.

Introduction

Fabricating inorganic materials with controllable morphology and crystalline superstructure is highly desired as their optical, electronic, magnetic, catalytic or biomedical properties are strongly morphology/structure-dependent.[1-4] For example, $CaCO_3$ in the shape of mushroom, dumbbell, flower, and truncated-octahedron has been applied in toothpastes, cosmetics and water treatment,[5] while $CaCO_3$ nanocrystals with porous or hollow structure have served as drug carriers.[6, 7]

Alpha-calcium sulfate hemihydrate (α-HH), an important class of cementitious minerals, has been widely used in molding, construction industry, bone repair,[8] dentistry odontology[9] and drug delivery[10] due to its excellent workability, high strength, biocompatibility and biodegradability.[4,11] The structure, morphology and size of α-HH often determine its properties and functionalities. For instance, α-HH wires and whiskers have been used as reinforcing agent in polymer and ceramic composites due to their good thermal stability and compatibility.[12] In comparison, α-HH particles with a low aspect ratio or spherical shape possess better injectability and mechanical properties after hydration, and are preferable for use as bone cements.[13,14] On the other hand, micro-scale α-HH single crystals are mainly used as ceramic molds, building materials and bone-substitute materials, while the nano-scale α-HH polycrystals can promisingly serve as drug carriers and find other medical applications,[15] thus highlighting the importance of structure and morphology control of α-HH.

Up to the present, long columns, rods, wires, whiskers, and nanoparticles[16-18] of α-HH have been produced in autoclave, electrolyte solution, microemulsion and reverse microemulsion.[19-21] Many strategies have been developed to regulate the size and morphology of α-HH, for instance, adjusting electrolyte concentration and the use of modifier.[22,23] These researches mostly concentrate on the regulation of α-HH single crystalline wires, whiskers and rods,[18] which all accord with the growth habit of α-HH (1-D growth along the *c* axis).[24] Herein we report on the control of α-HH structure and morphology which do not follow its usual crystallization habits. In Na_2EDTA-contained ethylene glycol-water thermal-system, single/poly crystalline α-HH particles with controllable sizes and morphologies are obtained by simply adjusting the ratio of ethylene glycol to water (G/W). This work will offer new opportunities for the application of α-HH.

Experimental Section

Materials

Analytical grade $CaCl_2$, $(NH_4)_2SO_4$, and Na_2EDTA were all purchased from Sinopharm Chemical Reagent Co. Ltd., Shanghai, China. The ethylene glycol-water solution was prepared by deionized water and ethylene glycol (reagent

[a]*Department of Environmental Engineering, Zhejiang University, Hangzhou 310058, China.*
E-mail address: guanbaohong@zju.edu.cn Tel.: +86-0571-88982026; Fax: +86-0571-88982026.
[b]*Engineering Research Center for Waste Oil Recovery Technology and Equipment, Chongqing Technology and Business University, Chongqing 400067,China*
† Electronic supplementary information (ESI) available.

grade, Sinopharm Chemical Reagent Co. Ltd., Shanghai, China).

Synthesis of α-HH

The experiments were performed in a 100 ml Teflon reactor with constant magnetic stirring at the temperature of 95°C (with a deviation of ± 0.5°C).

In a typical procedure, precursor solution of Ca^{2+} was prepared by dissolving 222.0 mg $CaCl_2$ and 186.0 mg Na_2EDTA in 5.0 ml glycol, and SO_4^{2-} precursor solution was obtained by dissolving 264.0 mg $(NH_4)_2SO_4$, Na_2EDTA and ethylene glycol in water. The volume of $(NH_4)_2SO_4$ solution was fixed at 45 ml and the G/W was set at 0.4, 0.7, 1.5, 2.5, 5.0, 10.0, 15.0 and 50.0 in different experiments. The molar ratio of calcium ions to sulfate ions (Ca/S) was kept at 1.0. The two solutions were heated at the desired temperature to be transparent and then mixed immediately. After 30 min of reaction, the hot suspension was quickly vacuum filtered, washed with boiling water, rinsed with anhydrous ethanol for 3 times to remove water, ethylene glycol and mediating agent. Solid products were collected after dried at 60°C for 2 h.

Characterization

The solid products were subjected to the laser particle size analyzer (Mastersizer 2000, Malvern Instruments Ltd., Worcestershire, U.K.) for the measure of particle size distribution. The X-ray diffraction (XRD) was performed by a powder XRD analyzer (D/Max-2550 pc, Rigaku Inc., Tokyo, Japan) with Cu Kα radiation at a scanning rate of 8°/min in the 2θ range from 5° to 80° for the phase identification. The thermogravimetry and differential scanning calorimetry (TG-DSC, STA-409PC, NET-ZSCH, Germany) were conducted to distinguish α-HH from hemihydrate (HH) phases. The morphology was examined by the scanning electron microscopy (SEM, Hitaches-570, Japan). Transmission electron microscopy (TEM) images and selected-area electron diffraction (SAED) patterns were obtained on TEM (Titan Chemi STEM, USA) at an acceleration voltage of 200 kV. Fourier transform infrared (FTIR) spectra were recorded on a spectrometer (IRAffinity-1, Shimadzu, Japan) with a resolution of 4 cm^{-1} over the frequency range of 400 - w4000 cm^{-1}.

Results and Discussion

Control of α-HH morphology and microstructure

Calcium sulfate crystals were synthesized by simply mixing the ethylene glycol-water solutions of Ca^{2+} and SO_4^{2-} precursors in the presence of 10 mM Na_2EDTA at 95°C. The volume ratio of ethylene glycol to water (G/W) is found to play a key role in determining the phase and morphology of crystals at the fixed dosages of $CaCl_2$ and Na_2EDTA. The phase change of calcium sulfate with an increase in G/W from 0.7 to 2.5 was tracked by the XRD analysis (Supporting Information S1). At a low G/W of 0.4, a mixture of dihydrate (DH) and HH (the dominate phase) is detected. While at a G/W higher than 0.7, only HH is detected. The weight loss (about - 6.22 wt%) in TG analysis occurring at 35 - 200°C confirms the presence of pure α-calcium sulfate hemihydrate (α-HH) phase, based on the endothermic peak at 163°C and the exothermic peak at 185°C in the DSC curve (Supporting Information S2). The results thus indicate that a higher G/W favors the precipitation of the α-HH phase. In this system, the critical mole concentration of glycerol for DH - HH phase transition is found to be 12% (equal to G/W 0.55) at 85°C in the glycerol-water solution.[25] Consequently, α-HH becomes more stable and precipitates as a unique phase with the increase of ethylene glycol concentration.

The dependence of morphology on G/W is examined by SEM. At the G/W of 0.4, α-HH crystals precipitate in regular hexagonal prism shape with a length of ~ 8 μm and a width of ~ 3 μm (Figure 1a). As the G/W reaches 0.7, α-HH crystals with a short columnar prism shape slightly decrease in length to ~ 3 μm and keep the width of ~ 3 μm (Figure 1b). Flat-prisms of α-HH are obtained when the G/W goes up to 1.5, about 2 μm in length and 3 μm in width (Figure 1c). An increase in G/W to 2.5 results in the formation of crystals with a discoid-like morphology and a length of ~ 0.3 μm (Figure 1d). These observations suggest that an increase in G/W reduces the aspect ratio of α-HH from 2.7 to 0.1 for the prism-like α-HH crystals. When the G/W is further raised to 5.0, α-HH precipitates in microsphere shape with a diameter of ~ 2 μm (Figure 1e), a quite different shape from those under lower G/W. At G/W of 10, α-HH presents in ellipsoidal particles with a length of ~ 1.5 μm, a width about 1.0 μm and the aspect ratio of 1.5 (Figure 1f). Upon a further raise of G/W to 15.0, α-HH particles show in smaller ellipsoids with ~ 700 nm in length and ~ 400 nm in width (Figure 1g). When the G/W reaches 50.0, the ellipsoids evolve to nanoparticles with a length around 300 nm and width

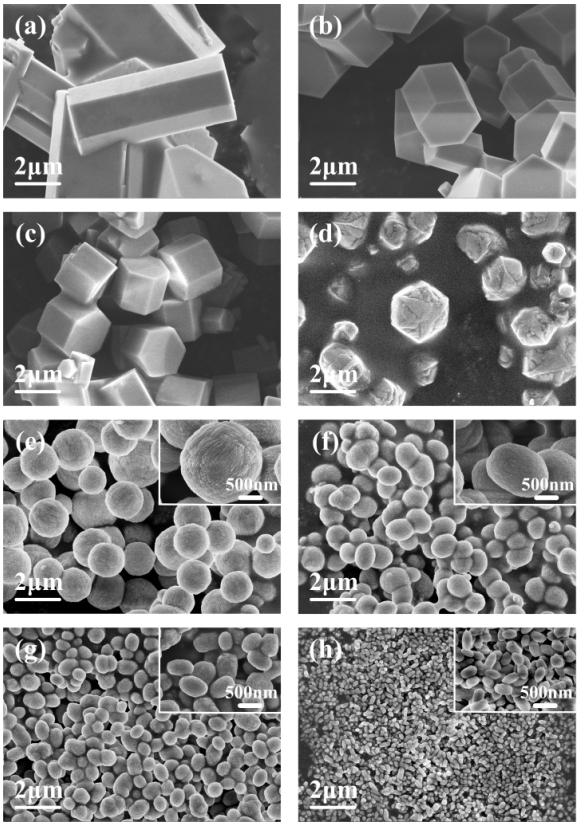

of ~ 150 nm (Figure 1h).

Figure 1. SEM images of α-HH synthesized at 95°C in ethylene glycol aqueous solutions with different G/Ws at: (a) 0.4, (b) 0.7, (c) 1.5, (d) 2.5, (e) 5.0, (f) 10.0, (g) 15.0 and (h) 50.0.

Considering the dramatic change in the morphologies of α-HH from prism to microsphere, TEM, SAED, and high-resolution TEM (HRTEM) were performed to further investigate the microstructure. Figure 2a shows the TEM image of α-HH crystal in regular hexagonal prism shape. The interplanar spacing of the lattice fringes is 0.603 nm in the HRTEM image (Figure 2b), corresponding to the (002) plane (0.603 nm) indicating that the α-HH is single-crystalline and predominately grow along the (001) direction. The inset SAED pattern (Figure 2b) can be indexed to the [1$\bar{1}$0] zone axis of α-HH and the indexes of the spots in the SAED pattern imply the preferential orientation of α-HH along the *c* axis. In Figure 2c, the TEM image reveals that the microsphere is not completely hollow. The HRTEM image and the inset SAED pattern confirm that the microspheres are polycrystalline (Figure 2d). The bright and intact diffraction ring suggests the nanocrystallines within the spheres are randomly organized. The values of the *d* spacing obtained from the diffraction ring of α-HH are 0.347, 0.280, 0.214 nm, corresponding to the (013), (-411) and (503) planes. These results demonstrate that α-HH develops into an uncommon spherical shape and a polycrystalline crystalline structure when G/W is higher than a threshold value.

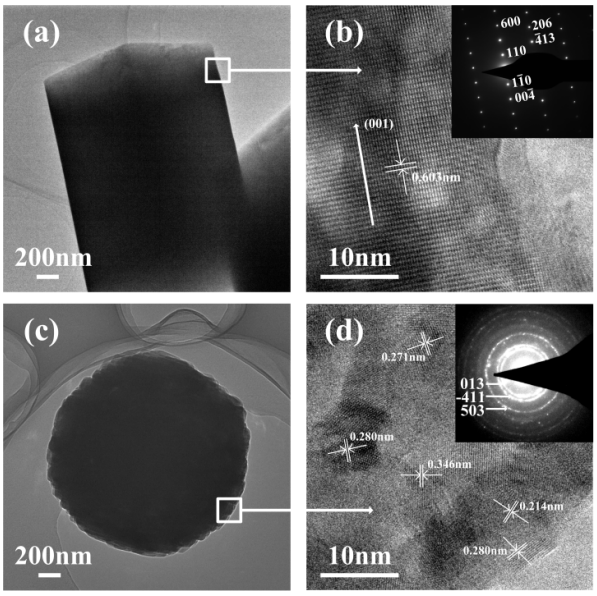

Figure 2. TEM images of α-HH synthesized at 95°C in ethylene glycol aqueous solutions with different G/Ws at (a) 0.7, (b) 5.0. HRTEM images and SAED patterns (inset) of α-HH synthesized at 95°C with different G/Ws at (c) 0.7 and (d) 5.0.

Effect of $CaCl_2$

To have an insight into the mechanism of morphology and microstructure evolution of α-HH with G/W, we changed the precursor concentration (denoted by $CaCl_2$ concentration below and the Ca/S of 1.0) in the presence of 10 mM Na_2EDTA at a fixed G/W of 5.0. At a low $CaCl_2$ concentration of 10 mM, α-HH crystallizes into prisms with flakes on surface (Figure 3a). Upon an increase of $CaCl_2$ concentration to 20 mM, nanosized spherical α-HH polycrystals form with diameter of about 800 nm covered by thin sheets on the surfaces (Figure 3b). α-HH polycrystalline spheres with smooth surfaces appear under 40 mM $CaCl_2$ (Figure 3c). With the concentration increasing to 60 mM, α-HH appears as microspheres with rough appearance and uneven size distribution (Figure 3d). At a certain G/W, the precursor concentration determines the supersaturation and a higher $CaCl_2$ concentration will generate a higher supersaturation.[26] A lower supersaturation usually provides a weak nucleating driving force, and leads to a slower crystal nucleation and growth rate, giving rise to the precipitation of α-HH in prism shape. With the increase of supersaturation, the rapid nucleation rate boosts a large number of nuclei,[27] resulting in the formation of polycrystals. Obviously, the supersaturation at 20 mM $CaCl_2$ is not high enough to form the regular sphere by producing sufficient nucleus instantly. The remained free ions are further consumed in the later crystal growth, leading to the formation of flakes attached to surfaces of the nanospheres. The 40 mM of $CaCl_2$ provides rational supersaturation for the formation of α-HH polycrystalline microsphere with smooth surfaces. The excessive supersaturation at 60 mM $CaCl_2$ is adverse to the sphericity and uniformity of α-HH polycrystalline microspheres due to the high nucleation rate over the self-assembly control by Na_2EDTA.

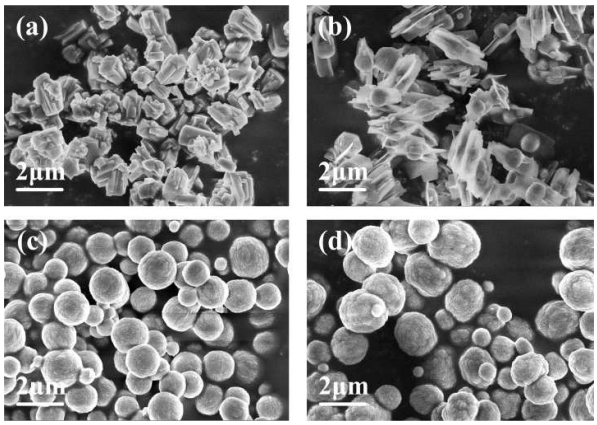

Figure 3. SEM images of α-HH synthesized under Na_2EDTA concentration of 10 mM and G/W of 5.0 at 95°C with different $CaCl_2$ concentrations at (a) 10 mM, (b) 20 mM, (c) 40 mM and (d) 60 mM.

Effect of Na_2EDTA

The dependence of morphology on the concentration of Na_2EDTA was examined at $CaCl_2$ concentration of 40 mM and G/W of 5.0. Without Na_2EDTA, α-HH whisks precipitate with a length of 5 - 8 μm (Figure 4a). In the presence of 1.25 mM Na_2EDTA, α-HH crystallizes as nanosized particles and the subunits then assemble into a bowknot-like structure (Figure 4b). With a further rising of Na_2EDTA concentration to 2.5 mM, the nano α-HH crystals assemble into rough potato-like microellipsoids with length of ~ 2.5 μm and width of ~ 1.5 μm

(Figure 4c). At 5.0 mM of Na_2EDTA, α-HH polycrystals appear in microsphere shape with rough surfaces and a diameter of 2 μm (Figure 4d). When the Na_2EDTA reaches 10 mM, α-HH polycrystals grow into perfect spheres with smooth surfaces of 2 μm in diameter (Figure 4e). Upon a further increase of Na_2EDTA to 20.0 mM, α-HH microspheres get smaller and some of them are covered by radial arranged flakes (Figure 4f).

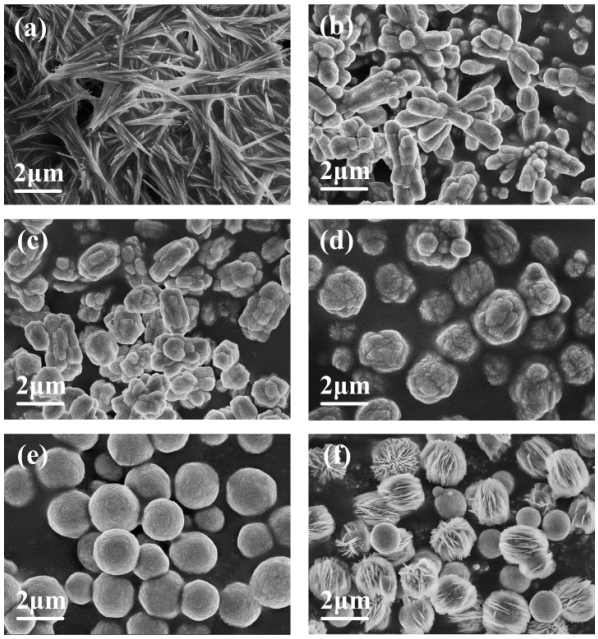

Figure 4. SEM images of α-HH synthesized under $CaCl_2$ concentration of 40 mM and G/W of 5.0 at 95°C with different Na_2EDTA concentrations at (a) 0 mM, (b) 1.25 mM, (c) 2.5 mM, (d) 5 mM, (e) 10 mM and (f) 20 mM.

As an anisotropic crystal, α-HH shows distinct growth rates at different crystal planes. The crystal lattice of α-HH consists of -Ca-SO_4-Ca-SO_4-Ca- chains with repeating, ionically bonded Ca and SO_4 ions, which forms a framework with continuous channels parallel to the *c* axis and favors the preferential 1D growth along the *c* axis.[24,28] Thus without Na_2EDTA, α-HH whiskers are obtained, which consists with its crystallization habit. The crystallization process changes upon the addition of Na_2EDTA. A similar phenomenon was reported in the self-assembled carbonated hydroxyapatite synthesis controlled by Na_2EDTA and bubble-template.[29] At concentration of 10 mM, the influence of Na_2EDTA becomes prominent and better than the lower ones, as evidenced by the bowknot-like particles and irregular spheres (Figure b-d). The spheres covered by a layer of thin sheets obtained at 40 mM $CaCl_2$ and 20 mM Na_2EDTA (Figure 4f) is similar as those formed at 20 mM $CaCl_2$ and 10 mM Na_2EDTA (Figure 3b), indicating that the excessive amount of Na_2EDTA decreases the supersaturation by chelating with of Ca^{2+} ions.[15] In general, as the Na_2EDTA concentration is raised, the monodispersity and smoothness of α-HH polycrystalline microspheres get better and then deteriorate. There is an optimal Na_2EDTA concentration for the formation of delicate particles under a fixed $CaCl_2$ concentration and G/W.

Growth mechanism of α-HH

The particle size distributions of α-HH particles synthesized at G/W from 5.0 to 50.0 illustrate that the microspheres and ellipsoids are monodisperse and can be characterized by a lognormal function (Figure 5). The surface weighted mean *D* are 0.4 μm, 0.8 μm, 1.3 μm and 2.2 μm, respectively. The corresponding crystalline sizes estimated from the broadened diffraction peaks with the Scherrer Equation are 10.96 nm, 17.81 nm, 20.65 nm, 34.75 nm, which coincide with SEM images taken at a high magnification (Figure 1 e-h). Increasing G/W leads to the size decrease of the particles as well as the nano-subunits, indicating that the increase of G/W promotes the supersaturation and accelerates the nucleation rate owing to the presence of a co-solvent in the solution which affects the activity coefficients and the solubility of the salt. Flaten[30] also pointed that the activity-based supersaturation increased as the ethylene glycol concentration was elevated. That is, the increase of G/W leads to elevation of supersaturation and then changes the crystal size and structure.

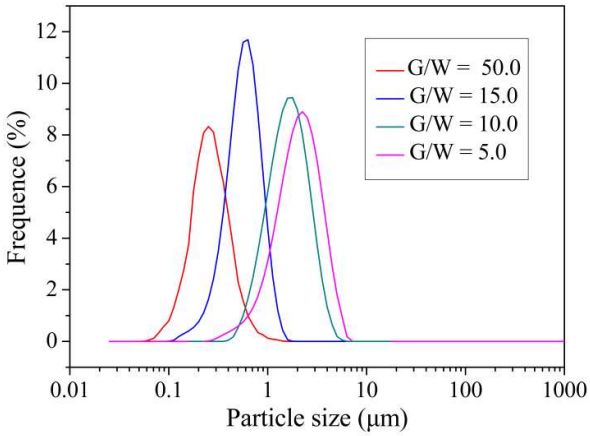

Figure 5. Particle size distributions of α-HH particles synthesized at 95°C with G/Ws at 5.0, 10.0, 15.0 and 50.0.

α-HH particles obtained at a low G/W of 0.7 and a high G/W of 5.0 were analyzed by FTIR (Supporting information S3). The two sharp peaks at 1400 and 1621 cm^{-1} assigned to COO^- stretching modes indicate the presence of Na_2EDTA in both the single crystalline and polycrystalline particles. Na_2EDTA is supposed to modify the morphology of single crystals by the preferential adsorption onto different crystal facets which control its growth rates along different crystal axes.[31] According to Hou's work,[32] the ratio of Ca^{2+} to SO_4^{2-} on the side facets as (200), (400), (020), and the top facets as (001) were 0.79, 0.79, 0.91, and 1.19, respectively. The crystals also have electrostatic charge imparted by the dipole on water molecules resulted from the preferred orientation. The denser distribution of Ca^{2+} ions on the top facets as (001) indicates they are more positively charged compared with the side facets. As a chelator of Ca^{2+}, EDTA ions with four groups of –COO- are expected to preferentially adsorb on the top facets as (001) and interact strongly with Ca^{2+} to lower the surface free energy.[33, 34] The growth is then hindered along the *c* axis and α-

HH crystals have the tendency to minimize the surface area covered by the side facets.

During the formation process of polycrystalline particles, the supersaturation determines the number and size of primary building blocks by regulating the nucleation kinetics.[35] Na_2EDTA mediates the assembly of α-HH domains, which at the same time serves as stabilizer. When the G/W increases from 5.0 to 50.0, the enhanced supersaturation produces more and smaller nuclei of α-HH. Therefore, only in the presence of strong stabilizing effect of Na_2EDTA, the polycrystalline microspheres form in uniform size with smooth surface. Obviously increasing G/W enhances the activity of Na_2EDTA to constrain the single crystal growth along *c* axis at a lower G/W and regulate the nanocrystals assembly as well as stabilize the polycrystals at a higher G/W.

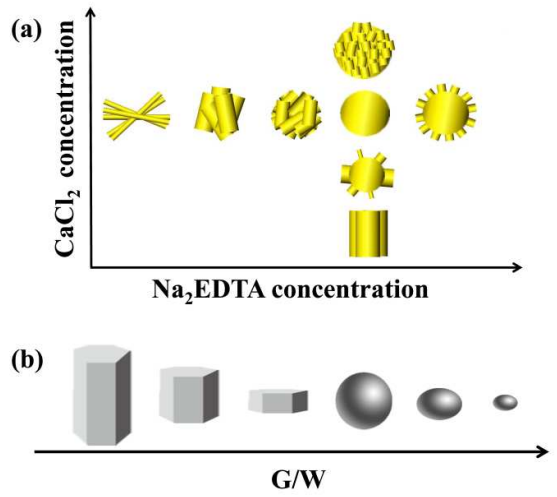

Figure 6. Schematic diagram of the structure and morphology evolution of α-HH particles with different (a) the concentration of $CaCl_2$ and Na_2EDTA and (b) G/W.

The structure and morphology evolution with the $CaCl_2$ and Na_2EDTA is illustrated in Figure 6a. Both $CaCl_2$ and Na_2EDTA have an optimum concentration for the formation of perfect polycrystalline microspheres at a fixed G/W. Figure 6b shows that the increase of G/W promotes supersaturation for α-HH precipitation and improves the influence of Na_2EDTA in the control of α-HH morphology, which is similar to the effect resulted from the concentration increase of both $CaCl_2$ and Na_2EDTA. Hence the desired morphology of α-HH single crystals or polycrystals can be obtained by adjusting G/W. The relationship is helpful in predicting the morphology under other experimental conditions. For example, when $CaCl_2$ concentration is 60 mM (higher than the optimum) in the presence of 10 mM Na_2EDTA at G/W 5.0, the resultant particles are defective spheres with rough surfaces (Figure 3d). The formation of smaller and more regular spheres with smooth surfaces is expected by raising Na_2EDTA concentration. We have performed further experiments to verify the mechanism. When Na_2EDTA concentration is raised to 20 mM, spheres with a diameter of ~ 1.4 μm are received (Supporting information S4). However, the particle size is more broadly distributed when compared with those synthesized at high G/W. Actually ethylene glycol aqueous solution offers an environment to produce more uniform crystals. Single crystals and polycrystals can be regulated only by adjusting G/W.

Conclusions

We have demonstrated an efficient method to synthesize nano/micro α-HH particles with controlled crystalline structure (single crystalline/polycrystalline) and morphology (hexagonal prism, discoid, sphere and ellipsoid) in Na_2EDTA-contained ethylene glycol aqueous solution by simply tuning the G/W. The elevation of G/W promotes the supersaturation for α-HH, leading to the precipitation from monocrystals to polycrystals due to the increase in nucleation rate and enhanced the activity of Na_2EDTA. At a low G/W, Na_2EDTA only constrains the growth of α-HH monocrystals along *c* axis to lower the aspect ratio through preferential adsorption. At a high G/W, Na_2EDTA mediates the self-assembly process of nanoparticle and stabilizes the polycrystals. This facile method provides opportunities for multiple applications of α-HH and paves a way to the controllable synthesis of single crystals and polycrystals.

Acknowledgements

We gratefully appreciate Project 21176219 supported by National Science Foundation of China and Changjiang Scholar Incentive Program (Ministry of Education, China, 2009).

References

1. X. Peng, L. Manna, W. Yang, J. Wickham, E. Scher, A. Kadavanich and A. P. Alivisatos, *Nature*, 2000, **404**, 59-61.
2. C. Burda, X. Chen, R. Narayanan and M. A. El-Sayed, *Chem. Rev.*, 2005, **105**, 1025-1102.
3. R. Bhargava, D. Gallagher, X. Hong and A. Nurmikko, *Phys. Rev. Lett.*, 1994, **72**, 416-418.
4. Z. B. Li, G and P. Demopoulos, *Ind. Eng. Chem. Res.*, 2006, **45**, 4517-4524.
5. J. Xiang, H. Cao, J. H. Warner and A. A. Watt, *Cryst. Growth Des.*, 2008, **8**, 4583-4588.
6. L. Qi, J. Li and J. Ma, *Adv. Mater.*, 2002, **14**, 300-303.
7. W. Wei, G. H. Ma, G. Hu, D. Yu, T. Mcleish, Z. G. Su and Z. Y. Shen, *J. Am. Chem. Soc.*, 2008, **130**, 15808-15810.
8. M. Cabanas, L. Rodriguez-Lorenzo and M. Vallet-Regi, *Chem. Mater.*, 2002, **14**, 3550-3555.
9. X. Han, H. Liu, D. Wang, F. Su, Y. Zhang, W. Zhou, S. Li and R. Yang, *Clin. Implant Dent. Relat. Res.*, 2013, **15**, 390-401.
10. J. C. Doadrio, D. Arcos, M. V. Cabañas and M. Vallet-Regí, *Biomaterials*, 2004, **25**, 2629-2635.
11. M. A. Rauschmann, T. A. Wichelhaus, V. Stirnal, E. Dingeldein, L. Zichner, R. Schnettler and V. Alt, *Biomaterials*, 2005, **26**, 2677-2684.
12. A. Y. Xu, H. P. Li, K. B. Luo and L. Xiang, *Res. Chem. Intermed.*, 2011, **37**, 449-455.
13. T. Feldmann, G. P. Demopoulos, *J. Cryst. Growth.*, 2012, **351**, 9-18.
14. P. Wang, E. J. Lee, C. S. Park, B. H. Yoon, D. S. Shin, H. E. Kim, Y. H. Koh and S. H. Park, *J. Am. Ceram. Soc.*, 2008, **91**, 2039-2042.
15. G. Jiang, Q. Chen, C. Jia, S. Zhang, Z. Wu and B. Guan, *Phys.*

Chem. Chem. Phys., 2015, **17**, 11509-11515.
16. B. Kong, B. Guan, M. Z. Yates and Z. Wu, *Langmuir*, 2012, **28**, 14137-14142.
17. X. Song, S. Sun, W. Fan and H. Yu, *J. Mater. Chem.*, 2003, **13**, 1817.
18. Y. Chen, Q. Wu and Y. Ding, *Eur. J. Inorg. Chem.*, 2007, **2007**, 4906-4910.
19. H. Fu, B. Guan, G. Jiang, M. Z. Yates and Z. Wu, *Cryst. Growth Des.*, 2012, **12**, 1388-1394.
20. L. Li, Y. J. Zhu and M. G. Ma, *Mater. Lett.*, 2008, **62**, 4552-4554.
21. D. W. Kirk, S. Tong, Patents: US 5562892 A, 1996.
22. F. Li, J. Liu, G. Yang, Z. Pan, X. Ni, H. Xu and Q. Huang, *J. Cryst. Growth*, 2013, **374**, 31-36.
23. C. Hazra, S. Bari, D. Kundu, A. Chaudhari, S. Mishra and A. Chatterjee, *Ultrason. Sonochem.*, 2014, **21**, 1117-1131.
24. C. Bezou, A. Nonat, J. C. Mutin, A. N. Christensen and M. Lehmann, *J. Solid State Chem.*, 1995, **117**, 165-176.
25. B. Guan, G. Jiang, H. Fu, L. Yang and Z. Wu, *Ind. Eng. Chem. Res.*, 2011, **50**, 13561-13567.
26. B. Guan, L. Yang and Z. Wu, *Ind. Eng. Chem. Res.*, 2010, **49**, 5569-5574.
27. A. N. Kulak, P. Iddon, Y. Li, S. P. Armes, H. Cölfen, O. Paris, R. M. Wilson and F. C. Meldrum, *J. Am. Chem. Soc.*, 2007, **129**, 3729-3736.
28. P. Ballirano, A. Maras, S. Meloni and R. Caminiti, *Eur. J. Mineral.*, 2001, **13**, 985-993.
29. X. Cheng, Z. Huang, J. Li, Y. Liu, C. Chen, R. a. Chi and Y. Hu, *Cryst. Growth Des.*, 2010, **10**, 1180-1188.
30. E. M. Flaten, M Seiersten and J. P. Andreassen, *J. Cryst. Growth,* 2009, **311**, 3533-3538.
31. C. J. Murphy, *Science*, 2002, **298**, 2139-2141.
32. S. Hou, J. Wang, X. Wang, H. Chen and L. Xiang, *Langmuir*, 2014, **30**, 9804-9810.
33. M. Auffan, J. Rose, O. Proux, D. Borschneck, A. Masion, P. Chaurand, J.-L. Hazemann, C. Chaneac, J. P. Jolivet and M. R. Wiesner, *Langmuir*, 2008, **24**, 3215-3222.
34. D. Kim, U. Gösele and M. Zacharias, *J. Cryst. Growth*, 2009, **311**, 3216-3219.
35. O. Söhnel and J. W. Mullin, *J. Colloid Interface Sci.*, 1988, **123**, 43-50.

Table of Contents

A facile method to control the structure and morphology of α-calcium sulfate hemihydrate

Qiaoshan Chen,[a] Guangming Jiang,[b] Caiyun Jia,[a] Hao Wang[a] and Baohong Guan[a,*]

† Department of Environmental Engineering, Zhejiang University, Hangzhou 310058, China

‡ Engineering Research Center for Waste Oil Recovery Technology and Equipment, Chongqing Technology and Business University, Chongqing 400067,China

*Corresponding author. Tel.: +86-0571-88982026; Fax: +86-0571-88982026.

E-mail address: guanbaohong@zju.edu.cn

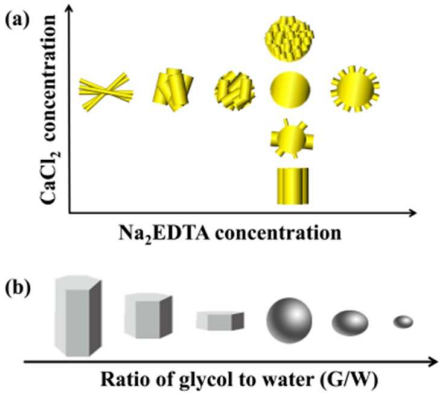

Synopsis: Synergy effect of $CaCl_2$ and Na_2EDTA on the structure and morphology control of α-HH by regulating G/W.